Towards a Reconfigurable Metacavity Antenna for Computational Imaging and DoA Estimation

Mengran Zhao*†, Luyi Wang†, Shitao Zhu†, Muhammad Ali Babar Abbasi*,
Thomas Fromenteze§, and Okan Yurduseven*
*Center for Wireless Innovation, ECIT, Queen's University Belfast, BT3 9DT Belfast, UK
†School of Information and Communication Engineering, Xi'an Jiaotong University, 710049 Xi'an, China
§Xlim Research Institute, University of Limoges, 87060 Limoges, France
mengran.zhao@qub.ac.uk

***Abstract*—In this paper, a reconfigurable metacavity antenna (RMA) that can be used for microwave computational imaging (CI) and direction of arrival (DoA) estimation applications is proposed. The RMA is an electrically over-sized metacavity with its back wall replaced by a 1-bit reconfigurable metasurface and its top surface etched with leaky circular irises. By leveraging the *frequency-diversity* and the *dynamic aperture* techniques, spatio-temporally low-correlated radiation patterns can be generated by the RMA at different operating frequencies and under different PIN states. The reflection coefficients at operating frequencies are under -10 dB, indicating the RMA is impedance-matched. The correlation coefficients are smaller than 0.3 and the singular values are close to each other, which demonstrates the spatial-orthogonality of the measurement modes. Simulated experiments are implemented to validate the feasibility of the proposed RMA for CI and DoA estimation. Using the developed RMA, the target image has been reconstructed and the far-field source has been estimated. The proposed design is validated through simulations in CST Microwave Studio.**

***Index Terms*—reconfigurable, metacavity, computational imaging, DoA estimation.**

I. Introduction

Conventionally, microwave imaging and direction of arrival (DoA) estimation require an antenna array at the receiver to capture the channel information [1]–[7]. According to the Fourier theory, spatial resolution depends on the dimensions of the radiating aperture, which should be sampled on a sub-wavelength scale to avoid aliasing. Receiver synchronization requires each antenna to be associated with an active chain to achieve beamforming. However, this multi-pixel layout exhibits notable constraints, such as increased data acquisition time and complex hardware architecture.

Recently, compressive sensing (CS) has gained significant traction, particularly in computational imaging (CI) [8]–[14] and DoA estimation [15]–[19]. Within the CS framework, the compressive single-pixel antenna radiating spatio-temporally varying field patterns plays a crucial role in facilitating these paradigms. The information can be encoded by a series of different radiation patterns and compressed into a single channel. Consequently, the requirement of raster scanning is eliminated, which can dramatically reduce the hardware complexity and the number of data acquisition channels.

Unlike the array-based method, the CS method leverages the spatio-temporally low-correlated radiation patterns to encode the scene information. The metasurface-based apertures have been proven qualified to generate these types of radiation patterns. The design is typically achieved using two techniques known as *frequency-diversity* [9]–[11] and *dynamic aperture* [17]–[19]. The frequency-diversity technique controls the variation of radiation patterns by a simple frequency sweep and facilitates probing the targets or far-field sources. The dynamic aperture approach relies on loading the metasurface aperture with reconfigurable elements, such as PIN diodes, and manipulating them to synthesize diverse radiated fields. The dynamic aperture eliminates the need for a large operating bandwidth posed by the frequency-diversity, which can further simplify the hardware architecture due to its single-frequency operation ability.

In this paper, a reconfigurable metacavity antenna (RMA) that can be used for both CI and DoA estimation applications is proposed. The proposed RMA is an electrically over-sized metacavity with its back wall replaced by a 1-bit reconfigurable metasurface and its top surface etched with leaky circular irises. The generated radiation patterns are low-correlated either at different frequencies or under different PIN states (i.e., *on* and *off*), which satisfies the CS applications.

The rest of this paper is organized as follows. In Section II, the RMA-based CI and DoA estimation concepts and processes are introduced. In Section III, the 1-bit reconfigurable metasurface and the circular iris exhibiting broadband radiation characteristic are designed. The performance of the proposed RMA including the reflection coefficient (S_{11}), the singular values (SVs), and the correlation coefficients (CCs) of measurement modes are also evaluated. In Section IV and Section V, the RMA-based CI and DoA estimation experiments are carried out in the CST Microwave Studio (MWS) software, respectively. Desired results (i.e., reconstruction of the target image and estimation of the far-field source) are obtained. In Section VI, conclusions are summarized.

II. RMA-based CI and DoA estimation

A. RMA-Based CI

In a RMA-based CI system, as shown in Fig. 1, the electric field generated by the transmitter (Tx) is used to illuminate the imaging scene and the scattered field is detected by the receiver (Rx) [8]–[12]. Considering the aforementioned process as a

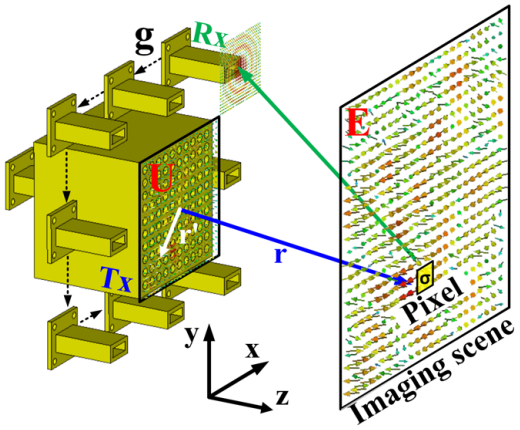

Fig. 1. Configuration of the RMA-based CI.

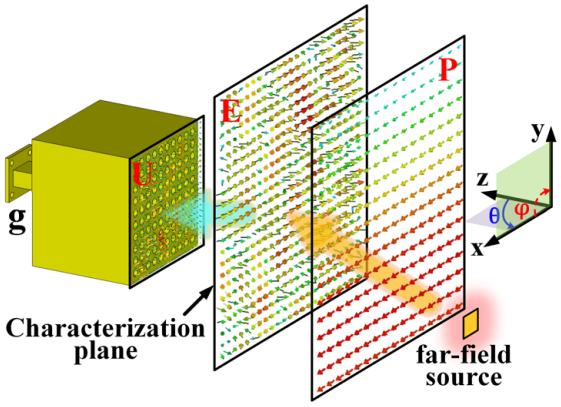

Fig. 2. Configuration of the RMA-based DoA estimation.

scalar problem, the signal measured at frequency f under PIN state s can be expressed as:

$$g(f,s) = \int_V E_T(\vec{r},f,s)\sigma(\vec{r})E_R(\vec{r},f,s)^T dV \tag{1}$$

where $E(\vec{r},f,s) = U(\vec{r'},f,s)G(\vec{r'},\vec{r},f)$ denotes the radiated fields at the imaging scene, $\sigma(\vec{r})$ refers to the imaging scene scattering coefficient, $\vec{r}$ represents the position vector from the origin to an imaging pixel, and $[\cdot]^T$ is the transpose operation [9]. Here, $U(\vec{r'},f,s)$ denotes the aperture field, $\vec{r'}$ represents the element position vector. $G(\vec{r'},\vec{r},f)$ is the Green's function, which is expressed as:

$$G(\vec{r'},\vec{r},f) = \frac{e^{-j\frac{2\pi f}{c}|\vec{r}-\vec{r'}|}}{4\pi|\vec{r}-\vec{r'}|} \tag{2}$$

where c is the light speed. According to the first Born approximation [20], the RMA-based CI process can be expressed as:

$$g(f_i,s_j) = \sum_{i=1}^{M}\sum_{j=1}^{N}\sum_{k=1}^{Q} E_T(\vec{r_k},f_i,s_j)\sigma(\vec{r_k})E_R(\vec{r_k},f_i,s_j)^T \tag{3}$$

where M, N, Q denote the number of operating frequencies, PIN states, and discrete scene pixels, respectively. The sensing matrix can be briefly defined as $H \in \mathbb{C}^{M,N\times Q}$ with $H_{ij,k} \propto E_{T_{ij,k}}E_{R_{ij,k}}$. The ill-conditioned inverse problem $\vec{g} = \vec{H}\vec{\sigma}$ can be solved efficiently using the least-squares (LS) algorithm to retrieve $\sigma(\vec{r})$ [8]–[11].

B. RMA-Based DoA Estimation

As shown in Fig. 2, the RMA-based DoA estimation shares some similarities with the RMA-based CI. However, these two problems are different at a fundamental level. The RMA-based CI focuses on the near-field operations and relies on the back-scattered measurements. The RMA-based DoA estimation, on the other hand, is a far-field problem and there is no apriori information about the source.

To implement the DoA estimation using the CI framework, a *characterization plane* is needed to compress the incident plane-wave excited by the far-field source. Essentially, our goal is to use the aperture field (U) on the characterization plane (E) to probe the P - far-field source projected patterns on the same characterization plane at the same set of frequencies. The P contains the propagation information of the far-field source, namely the incident angles (θ,φ). As shown in Fig. 2, a plane located in the near-field of the RMA is chosen as the characterization plane. The measurement modes radiated by the RMA are firstly calculated on this plane using $E(\vec{r},f,s) = U(\vec{r'},f,s)G(\vec{r'},\vec{r},f)$. The projection of the far-field source on this plane can be expressed as:

$$P(\vec{r},f) = e^{-j\frac{2\pi f}{c}(\hat{x}sin\theta cos\varphi + \hat{y}sin\theta sin\varphi)} \tag{4}$$

where (θ,φ) refer to the incident angles of the far-field source. The projected pattern is compressed into one channel by the measurement modes of RMA, and the measured signal $g(f,s)$ can be expressed as:

$$g(f,s) = \int_{\vec{r}} E(\vec{r},f,s)P(\vec{r},f)dr \tag{5}$$

Here, we note that (5) and (1) share the same form. Thus, the estimated projected pattern on the characterization plane (P_{est}) can be acquired by utilizing the aforementioned CI method. Then, the DoA pattern can be obtained by performing a Fourier transform operation $\mathcal{F}$. Finally, the incident angles (θ,φ) can be retrieved by using a peak-finding algorithm on the estimated DoA pattern [15]–[19].

III. Design of RMA

The aperture field of a RMA can be described as:

$$U(\vec{r_p'},f,s) = \sum_{p=1}^{P} A_p(\vec{r_p'},f)I(\vec{r_p'},f,s) \tag{6}$$

where $A_p(\vec{r_p'},f)$, referred to as the radiation factor (RF), represents the modulation of the p_{th} radiating structure at location $\vec{r_n'}$ and frequency f. The $I(\vec{r_p'},f,s)$, referred to as the excitation factor (EF), represents the source field projected onto the top surface of RMA at location $\vec{r_n'}$, frequency f and under PIN state s. In order to generate spatio-temporally

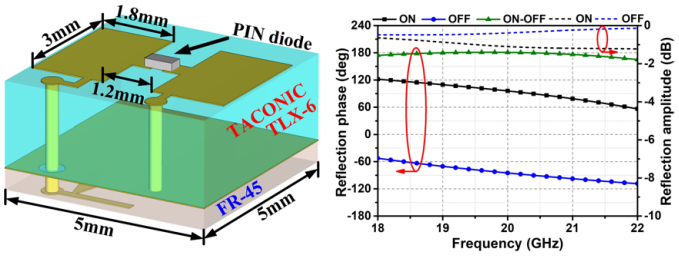

(a) (b)

Fig. 3. (a) Schematic of the 1-bit metamaterial element; (b) Reflection characteristic under the on and off working states.

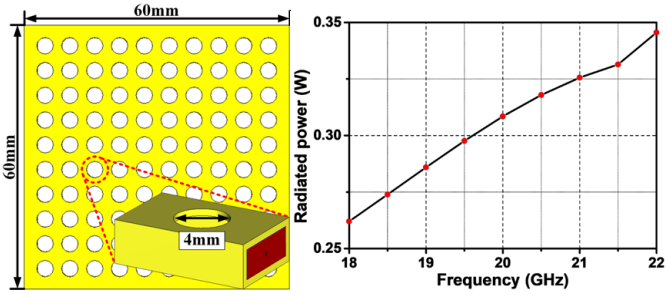

(a) (b)

Fig. 4. (a) Diagram of the leaky circular iris; (b) Radiation performance of the circular iris (with an input power of 0.5 W).

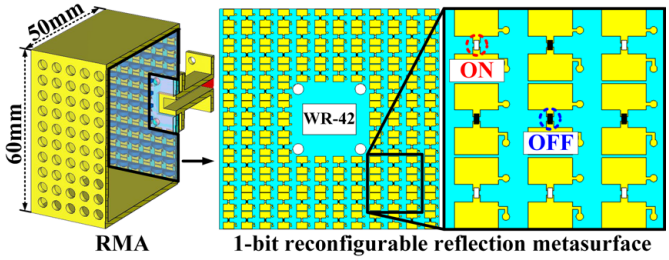

Fig. 5. Schematic of the RMA. Dimensions of the RMA are $4\lambda \times 4\lambda \times 3.34\lambda$ (length×width×height), where λ represents the wavelength at central frequency 20 GHz.

orthogonal radiation patterns, the RF and/or the EF should vary with the frequency and/or the PIN state. In this work, we focus on changing the EF to obtain diverse radiation patterns.

The proposed single-pixel RMA leverages the modulation of a 1-bit reconfigurable metasurface to generate diverse field distributions, thereby providing spatio-temporally varying EFs to the radiating structures. The main body of the RMA is an electrically over-sized cavity offering frequency-diverse field distributions [8], [9]. The reconfigurable metasurface is composed of 1-bit metamaterial elements, whose reflection phase is controlled by switching the on/off states of the loaded PIN diodes across the RMA aperture. The circular iris is used as the broadband radiating structure following our previous designs [9].

A. 1-Bit Metamaterial Element

A 1-bit metamaterial element should exhibit a 180° reflection phase difference corresponding to its on and off working state. In this paper, a sandwich-structured 1-bit metamaterial element as shown in Fig. 3(a) is proposed to constitute the reconfigurable metasurface. The upper and lower substrates are TLX-6 ($\epsilon_r = 2.65$) and FR-45 ($\epsilon_r = 4.5$) from TACONIC with the thickness of 2 mm and 0.5 mm, respectively.

From Fig. 3(b), the reflection phase difference between the on and off states remains stable at 180° across the frequency range of 18 to 22 GHz. Furthermore, the reflection amplitudes of both states are higher than -1.1 dB, which ensures a high reflection efficiency of the element.

B. Circular Iris Radiating Structure

For the RMA to function effectively in both the frequency-diverse and dynamic modes, it is essential for the radiating structure to be broadband. As shown in Fig. 4(a), a circular iris is used to couple energy from the metacavity and radiate. In order to enhance the diversity of EFs, the circular iris should work under low-efficiency to increase the number of reflections (i.e., modulation process) inside the metacavity. The performance of the circular iris is shown in Fig. 4(b). It is evident that the circular iris exhibits a balanced radiation response within the working bandwidth.

C. RMA and Performance Analyses

As shown in Fig. 5, the proposed RMA is an electrically over-sized metacavity with its back wall replaced by a 1-bit reconfigurable metasurface and its top surface etched with leaky circular irises. Different reflection responses are obtained when altering the PIN states of the 1-bit metamaterial elements, which lays a foundation for generating spatio-temporally diverse radiation patterns.

The performance of the proposed RMA is shown in Fig. 6. As shown in Fig. 6(a), the S_{11} is under -10 dB within the highlighted frequency bandwidths, indicating the impedance-match at these frequencies. Each line in Fig. 6(a) denotes a different PIN state. Here, for simplification, only 5 PIN states are shown. The SV curves of measurement modes under different conditions are shown in Fig. 6(b). In total 9 frequencies and 50 PIN states are selected, resulting in a maximum of 450 measurement modes. The CCs of measurement modes at different frequencies and under different PIN states are also calculated in Fig. 6(c) and 6(d). The average CC under two cases are 0.23 and 0.28, which is qualified to the CI and DoA estimation [10], [11].

IV. CI EXPERIMENTS

To verify the feasibility of the proposed RMA, the RMA-based CI experiments are firstly implemented in this section. As shown in Fig. 1, the RMA is used as Tx, a probe is used as Rx. The Rx can be moved to eight different positions to detect the measured signal g, which increases the number of useful measurement modes efficiently. The imaging scene is 20 cm×20 cm in both the x- and y-directions, and it is discretized into 81 (9×9) pixels with a side length of 2.5 cm. The target is

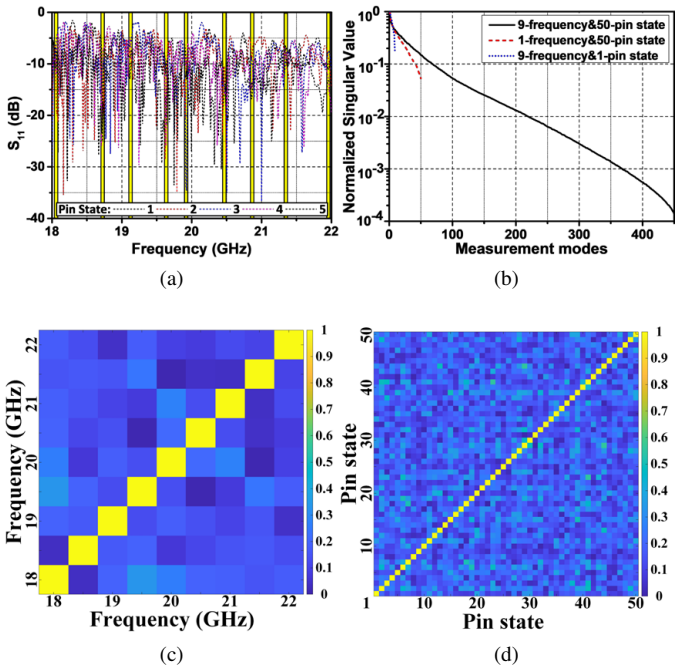

Fig. 6. The performance of the proposed RMA. (a) S_{11} ; (b) SVs; CCs (c) at 9 different frequencies; (d) under 50 different PIN states.

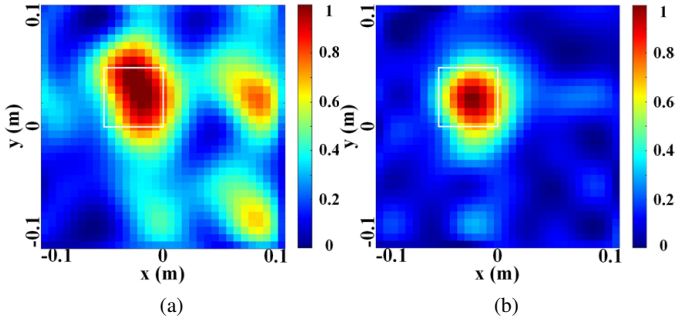

Fig. 7. Reconstructed target image from the (a) 9 frequency-diverse measurement modes; (b) 50 dynamic measurement modes.

a 5 cm metal square, centered at (x = -2.5 cm, y = 2.5 cm). The CI experiments are implemented with a signal-to-noise ration (SNR) of 20 dB.

As shown in Fig. 7, the target can be imaged using either the frequency-diversity or the dynamic aperture technique. However, better results are obtained using the dynamic aperture technique due to the more useful measurement modes it can generate.

V. DoA Estimation Experiment

The RMA-based DoA estimation experiment is then carried out in this section. As shown in Fig. 2, the single-pixel RMA is used to receive the measured signal g at 20 GHz. In this work , only the single-source scenario is considered for simplification. Nevertheless, it can be extended to a multi-source scenario by increasing the number of PIN states [19].

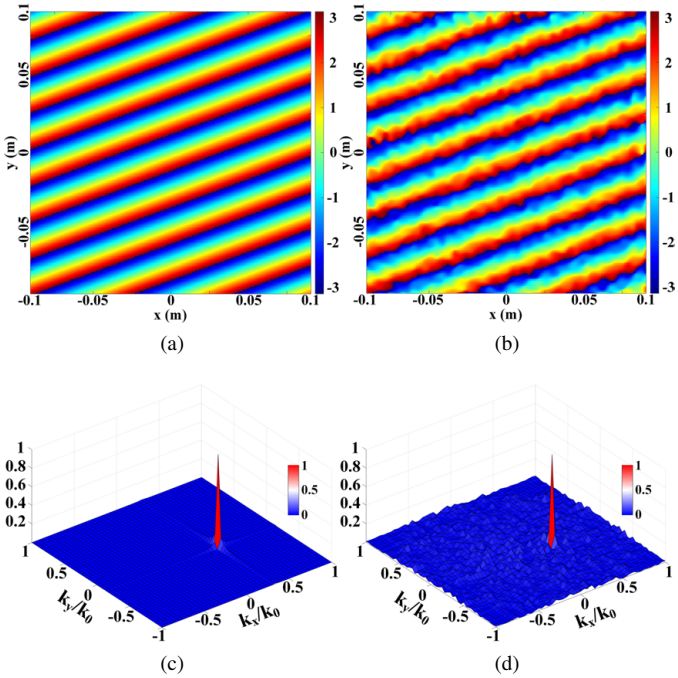

Fig. 8. CS-based DoA estimation results. (a) Original and (b) estimated projected patterns on the characterization plane; (c) Original and (d) estimated DoA patterns.

For this study, the incident angle of the source is set as ($\theta = 20°, \varphi = -20°$). The characterization plane is positioned at a distance of 0.2 m from the RMA aperture. The far-field source projection pattern (phase in radians) on the characterization plane and the original DoA pattern are shown in Fig. 8(a) and 8(c). The retrieved projection pattern on the characterization plane, P_{est}, is shown in Fig. 8(b). The estimated DoA pattern, $\mathcal{F}(P_{est})$, is shown in Fig. 8(d), from which can calculate the estimated incident angle ($\theta_{est}, \varphi_{est}$). Using a peak-finding algorithm in Fig. 8(d), the largest wave-vectors are found at $k_x/k_0 = sin\theta cos\varphi$ = 0.333 and $k_y/k_0 = sin\theta sin\varphi$ = -0.125, resulting in θ_{est} = 20.855°, φ_{est} = −20.556°, which is in good agreement with the ground truth ($\theta = 20°, \varphi = -20°$).

VI. Conclusion

In this paper, we presented a RMA that can be used for both CI and DoA estimation. The proposed RMA consists of an over-seized metacavity, a 1-bit reconfigurable metasurface and broadband circular irises. In total 450 spatio-temporally low-correlated measurement modes with CCs smaller than 0.3 were obtained under 9 discrete frequencies and 50 PIN states. To verify the feasibility of the designed RMA, CI and DoA estimation experiments were carried out. The target image was reconstructed and the incident angle of far-field source was estimated. The presented design exhibits significant potential for future hardware-efficient 6G communication systems with integrated sensing and communication (ISAC) capabilities.

ACKNOWLEDGMENT

This work was funded in part by the National Key R&D Program of China under Grant 2022YFB3902400, in part by the Natural Science Foundation of China under Grant 62071371 and in part by the Leverhulme Trust under Research Leadership Award under Grant RL-2019-019.

REFERENCES

[1] R. Appleby, R. N. Anderton, S. Price, N. A. Salmon, G. N. Sinclair, P. R. Coward, A. R. Barnes, P. D. Munday, M. Moore, A. H. Lettington, and D. A. Robertson, "Mechanically scanned real-time passive millimeter-wave imaging at 94 GHz," *in Proc. SPIE Passive Millimeter Wave Imag. Technol. VI Radar Sens. Technol. VII*, pp. 1-6, Aug. 2003.

[2] N. A. Salmon, "3-D radiometric aperture synthesis imaging," *IEEE Trans. Microw. Theory Techn.*, vol. 63, no. 11, pp. 3579-3587, Nov.2015.

[3] Z. Chen, G. Gokeda, and Y. Yu, *Introduction to direction-of-arrival estimation*, Artech, 2010.

[4] T. E. Tuncer and B. Friedlander,*Classical and modern direction-of-arrival estimation*, Academic Press, 2009.

[5] J. Chen, S. Guan, Y. Tong, and L. Yan, "Two-dimensional direction of arrival estimation for improved archimedean spiral array with MUSIC algorithm," *IEEE Access*, vol. 6, pp. 49740-49745, Aug. 2018.

[6] D. Smith, O. Yurduseven, B. Livingstone, and V. Schejbal, "Microwave imaging using indirect holographic techniques," *IEEE Antennas Propag. Mag.*, vol. 56, no. 1, pp. 104-117, Feb. 2014.

[7] M. Elsdon, O. Yurduseven, and D. Smith, "Early stage breast cancer detection using indirect microwave holography," *Prog. Electromagn. Res.*, vol.143, pp. 405-419, Nov. 2013.

[8] T. Sleasman, M. F. Imani, J. N. Gollub, and D. R. Smith, "Microwave imaging using a disordered cavity with a dynamically tunable impedance surface," *Phys. Rev. Appl.*, vol. 6, no. 5, pp. 054019, Nov. 2016.

[9] T. Fromenteze, O. Yurduseven, M. Boyarsky, J. Gollub, D. L. Marks, and D. R. Smith, "Computational polarimetric microwave imaging," *Opt. Express*, vol. 25, no. 22, pp. 27488-27505, Oct. 2017.

[10] M. Zhao, S. Zhu, X. Chen, J. Li, D. Hu, L. Wang and A. Zhang, "Frequency-diverse transmission metamaterial aperture with a bunching random beam," *IEEE Antennas Wirel. Propag. Lett.*, vol. 17, no. 6, pp. 1029-1033, Jun. 2018.

[11] M. Zhao, S. Zhu, J. Li, H. Shi, J. Chen, Y. He and A. Zhang, "Frequency-diverse bunching metamaterial antenna for coincidence imaging," *Materials*, vol. 12, no. 11, Jun. 2019, Art. no. 1817.

[12] M. F. Imani, J. N. Gollub, O. Yurduseven, A. V. Diebold, M. Boyarsky, T. Fromenteze, L. Pulido-Mancera, T. Sleasman, and D. R. Smith, "Review of metasurface antennas for computational microwave imaging," *IEEE Trans. Antennas Propag.*, vol. 68, no. 3, pp. 1860-1875, Mar. 2020.

[13] T. V. Hoang, V. Fusco, T. Fromenteze, and O. Yurduseven, " Computational polarimetric imaging using two-dimensional dynamic metasurface apertures," *IEEE Open J. Antennas Propag.*, vol. 2, pp. 488-497, Apr. 2021.

[14] M. Zhao, S. Zhu, H. Huang, D. Hu, X. Chen, J. Chen, and A. Zhang, "Frequency-diverse metamaterial cavity antenna for microwave coincidence imaging," *IEEE Antennas Wirel. Propag. Lett.*, vol. 20, no. 6, pp. 1103-1107, 2021.

[15] O. Yurduseven, M. A. B. Abbsi, T. Fromenteze, and V. F. Fusco, "Frequency-diverse computational direction of arrival technique," *Sci. Rep.*, vol. 9, no. 1, Nov. 2019, Art. no. 16704.

[16] M. A. B. Abbasi, V. F. Fusco, O. Yurduseven, and T. Fromenteze, "Frequency-diverse multimode millimetre-wave constant-ϵ_r lens-loaded cavity," *Sci. Rep.*, vol. 10, no. 1, Dec. 2020, Art. no. 22145.

[17] T. V. Hoang, R. Sharma, V. F. Fusco, and O. Yurduseven, "Single-pixel compressive direction of arrival estimation using programmable metasurface apertures," *in Proc. Passive and Active Millimeter-Wave Imaging XXIV*, vol. 11745, Apr. 2021, Art. no. 117450B.

[18] T. V. Hoang, V. F. Fusco, M. A. B. Abbsi and O. Yurduseven, "Single-pixel polarimetric direction of arrival estimation using programmable coding metasurface apertures," *Sci. Rep.*, vol. 11, no. 1, Dec. 2021, Art. no. 23830.

[19] O. Yurduseven, T. V. Hoang, M. A. B. Abbsi, and V. F. Fusco, "Compressive direction of arrival estimation with wave-chaotic antennas," in *Proc. 2022 PhotonIcs & Electromagnetics Research Symposium. (PIERS)*, Apr. 2022, pp. 403-408.

[20] J. Li, X. Wang, and T. Wang, "On the validity of born approximation," *Prog. Electromagn. Res.*, vol. 107, pp. 219-237, 2010.